

# JGR Atmospheres

## RESEARCH ARTICLE

10.1029/2019JD030954

### Key Points:

- Cloud overlap parameterization used to calculate the total cloud fraction (TCF) in climate models has still received far less attention
- Dynamical factors are proven able to develop overlap parameterization and reduce the TCF bias over SGP site compared with previous one
- Contribution calculation verifies that atmospheric instability contributes 70% of long-term variation of cloud overlap over SGP site

### Supporting Information:

- Supporting Information S1

### Correspondence to:

J. Huang,  
hjp@lzu.edu.cn

### Citation:

Li, J., Jian, B., Zhao, C., Zhao, Y., Wang, J., & Huang, J. (2019). Atmospheric instability dominates the long-term variation of cloud vertical overlap over the Southern Great Plains site. *Journal of Geophysical Research: Atmospheres*, 124. <https://doi.org/10.1029/2019JD030954>

Received 4 MAY 2019

Accepted 12 AUG 2019

Accepted article online 16 AUG 2019

## Atmospheric Instability Dominates the Long-Term Variation of Cloud Vertical Overlap Over the Southern Great Plains Site

Jiming Li<sup>1</sup> , Bida Jian<sup>1</sup>, Chuanfeng Zhao<sup>2</sup> , Yuxin Zhao<sup>1</sup>, Jing Wang<sup>1</sup>, and Jianping Huang<sup>1</sup> 

<sup>1</sup>Key Laboratory for Semi-Arid Climate Change of the Ministry of Education, College of Atmospheric Sciences, Lanzhou University, Lanzhou, China, <sup>2</sup>State Key Laboratory of Earth Surface Processes and Resource Ecology and College of Global Change and Earth System Science, Beijing Normal University, Beijing, China

**Abstract** Accurate representation of cloud vertical overlap in climate models is particularly significant for predicting the total cloud fraction (TCF) and calculating radiative budget. It refers to the parameterization of overlap parameter—decorrelation length scale  $L$ —but the potential of dynamical factors in developing parameterization of  $L$  has still received far less attention. Using ground-based radar observation over Atmospheric Radiation Measurement Southern Great Plains site, here long-term seasonal-averaged  $L$  is retrieved and shows a very high anticorrelation with TCF from different data sets, indicating that TCF is sensitive to the way of cloud overlap. Therefore, combined with meteorological reanalysis data set, a robust multiple regression model between  $L$  and dynamical factors is built and exhibits smaller TCF bias compared with previous parameterization of  $L$ . Contribution calculation further verifies that atmospheric instability contributes 70% of  $L$  variation, indicating that it dominates the long-term variation of  $L$  over Southern Great Plains site. This finding implies that dynamical factors should be taken into account in the parameterization of  $L$ .

**Plain Language Summary** The total cloud fraction plays a key role in modulating the Earth's radiation budget. Its calculation in atmospheric models involves many microphysical/dynamical processes and related parameterizations. One of the outstanding but less concerned challenges involves how to reasonably parameterize the cloud overlap parameter—decorrelation length scale  $L$  in these models. In this study, we demonstrate the potential of dynamical variables in developing the adjustable parameterization of  $L$ . By using the ground-based radar observations and meteorological reanalysis data set, the long-term climatology of  $L$  and a robust multiple regression model between  $L$  and dynamical factors are built. Statistical results indicate that new parameterization of  $L$  effectively reduces the bias of total cloud fraction compared with previous one. Such a long-term climatology of  $L$  is also enough to interpret the key issue of what factor dominates the long-term temporal variability of  $L$  over a fixed location. Here, we find that the atmospheric instability contributes 70% of  $L$  variation over SGP site. This finding implies that dynamical factors should be considered in the parameterization of  $L$ .

### 1. Introduction

Total cloud fraction (TCF) plays a key role in modulating the Earth's radiation budget (Jian et al., 2018; Seinfeld et al., 2016; Stephens, 2005). Its calculations in atmospheric models refer to many microphysical/dynamical processes and related parameterizations and thus contribute to one of the largest uncertainties in climate modeling when estimating and interpreting changes in the Earth's energy budget (Boucher et al., 2013). However, the challenges still remain even if cloud microphysical processes (e.g., condensate) are pretty well simulated, because atmospheric models have to make some assumptions about how the cloud layers overlap in the vertical direction, such as maximum, random, and minimum assumptions, to calculate the TCF (Geleyn & Hollingsworth, 1979; Weger et al., 1992). Previous studies have shown that these overlap assumptions may bias TCF calculations and lead to considerable differences in radiative budgets and heating/cooling rate profiles (Barker et al., 1999; Morcrette & Fouquart, 1986; Morcrette & Jakob, 2000; Pincus et al., 2005; Stephens et al., 2004; Wang et al., 2016). Thus, a more robust cloud overlap parameterization in climate models is imperative to improve the calculation of the radiative budgets.

Active sensors (e.g., lidar and radar) have been proven able to largely improve the treatment of cloud overlap behavior in the models and have thus been widely used to study the cloud overlap properties over different locations (e.g., Hogan & Illingworth, 2000; Huang et al., 2015; Li et al., 2018; Naud et al., 2008). Currently, the most widely used assumption is the exponential random overlap (Hogan & Illingworth, 2000), which expresses the mean observed cloud fraction between higher and lower cloud layers (hereafter,  $C_i$  and  $C_j$  are the cloud covers at higher and lower layers, respectively) as the linear combination of the maximum ( $C_{ij}^{\max} = \max\{C_i, C_j\}$ ) and random overlaps ( $C_{ij}^{\text{ran}} = C_i + C_j - C_i \times C_j$ ) in terms of an “overlap factor”  $\alpha$ :  $\alpha = (C_{ij}^{\text{obs}} - C_{ij}^{\text{ran}}) / (C_{ij}^{\max} - C_{ij}^{\text{ran}})$ . The overlap factor  $\alpha$  can be further fitted as an inverse exponential function of decorrelation length scale  $L$  and layer distance  $D$ ,  $\alpha = e^{-D/L}$ . Here, the cloud overlap parameters  $\alpha$  and  $L$  are both used to characterize the progressive transition from the maximum to random overlap assumption with increasing layer distances. Until now, many studies have verified the validity of the exponential random overlap using ground-based or spaceborne radar observations (e.g., di Giuseppe & Tompkins, 2015; Li et al., 2015; Mace & Bensonroth, 2002; Willén et al., 2005); however, they also found that the retrieved values of parameter  $L$  have wide ranges and vary with seasons, locations and spatiotemporal resolutions (e.g., Barker, 2008; Oreopoulos & Norris, 2011). Thus, an adjustable parameterization of  $L$  with some variables is better than a fixed  $L$ , such as the latitude-dependent scheme (Shonk et al., 2010), which parameterizes  $L$  as a function of latitude. In fact, the sensitivity of  $L$  to seasons and locations suggests that factors such as dynamical process or atmospheric state could be connected to the way cloud layers overlap. For example, a more unstable atmosphere during the summer season tends to favor a maximum overlap and larger decorrelation scales (e.g., Naud et al., 2008). As a result, recent studies have made a preliminary attempt to build statistical relationships between  $L$  and dynamical factors (e.g., wind shear or instability) by using spaceborne active observations (di Giuseppe & Tompkins, 2015; Li et al., 2018). However, the potential of dynamical variables that can be used to develop the parameterization of  $L$  has still received far less attention. In particular, the above studies only use short-term satellite observations and are insufficient to interpret the key issue of what factor dominates the long-term temporal variability of  $L$  over a fixed location.

To date, the Atmospheric Radiation Measurement (ARM; Ackerman & Stokes, 2003) program and related radar observations have performed well for 20 years. Based on the plentiful ground-based cloud properties and radiative flux observations over the SGP site, many studies have found that the cloud radiative effect highly correlates with TCF and thus verified the importance of accurate simulation of TCF in models (e.g., Dong et al., 2006; Dong & Mace, 2003). Delightedly, such a long-term ground-based radar observation also allows us to build long-term decorrelation length scale  $L$  climatology over a fixed site and further focuses on two key points: (1) how to parameterize  $L$  more reasonably and (2) what factor dominates the long-term temporal variability of  $L$  over a fixed location. The data and methods are described in section 2, the results and discussions are shown in section 3, and section 4 provides the summary.

## 2. Data Sets and Methods

### 2.1. Ground-Based Active Measurement

The ARM program Active Remote Sensing of Clouds (ARSCLs) Value-Added Product (VAP) for the SGP site (January 1997 to December 2010) is used to derive the long-term variation of cloud overlap properties over this site. This product combines radar reflectivities, and micropulse lidar returns to provide a continuous time series of the cloud vertical mask at 10-s and 45-m resolutions (Clothiaux et al., 2000). We use the parameters “ReflectivityBestEstimate” and “CloudBaseBestEstimate” to locate the atmospheric hydrometeors. For simplicity, this investigation defines the reflectivity values between  $-40$  and  $-10$  dBZ<sub>e</sub> as “cloud”; those profiles with reflectivity values larger than  $-10$  dBZ<sub>e</sub> are considered as “drizzle or precipitation” and eliminated from present analysis (Zhao et al., 2017). The CloudBaseBestEstimate parameter from lidar is used to provide the best estimate of cloud base height and assist in reducing the contamination of clutter (e.g., insects). Based on these limitations, a complete two-dimensional cloud mask can be generated at 10-s and 45-m resolutions. Because previous studies have pointed out that precipitation may bias cloud overlap statistics toward maximum overlap (di Giuseppe & Tompkins, 2015; Mace et al., 2009), we thus use the ground-based hourly precipitation measurements to further remove the cloud profiles during entire hours with precipitation (Naud et al., 2008). To match the hourly precipitation measurement, cloud cover profiles during 1 hr (e.g., about 360 profiles) are collected to generate the 1-hr averaged cloud cover profile.

Similar with previous studies (e.g., Mace & Bensonroth, 2002; Naud et al., 2008), we combine eight high-resolution (e.g., 45 m) vertical sublayers into one layer with 360-m resolution and consider this layer as “cloud layer” as long as any sublayer is cloudy. It possibly causes some potential uncertainties in retrieving the overlap parameter because the probability of a cloud occupying the layer increases with increasing grid spacing.

For each 1-hr averaged cloud cover profile, the overlap factor  $\alpha$  between any two atmospheric layers in this profile is calculated if the cloud covers ( $C_i$  and  $C_j$ ) of the two layers exceed 0 and their cloud top heights are both lower than 10.5 km (Naud et al., 2008). Ground-based radar observations have indicated that  $\alpha$  is sensitive to the spatial and temporal resolutions (e.g., Hogan & Illingworth, 2000; Mace & Bensonroth, 2002). Tompkins and Giuseppe (2015) have attributed this sensitivity to data truncation, where the overcast or single cloud layers are discarded from the samples when the sampling scale is smaller than the cloud system scale, thus biasing the calculation of overlap parameters and enhancing the sensitivity of overlap parameters to the spatial scale. Here, the sampling scale can be translated from the temporal resolution (e.g., 1 hr) and mean wind speed (Hogan & Illingworth, 2000). To reduce the sensitivity of  $\alpha$  to the spatial scale caused by data truncation, Tompkins and Giuseppe (2015) further suggested that the scenes with cloud cover exceeding 50% should be removed from the analysis when the sampling resolution is smaller than the cloud system scale. Although this simple cloud filter decreases the available sample number, the sensitivity of  $\alpha$  to the spatial resolution is largely reduced. Following their suggestion, we apply an upper limit of cloud cover (50%; i.e.,  $0.0 < C_i < 0.5$  and  $0.0 < C_j < 0.5$ ) at any atmospheric layer, instead of 100%, to perform the calculation of  $\alpha$  based on the equation:  $\alpha = (C_{ij}^{\text{obs}} - C_{ij}^{\text{ran}}) / (C_{ij}^{\text{max}} - C_{ij}^{\text{ran}})$ . To ensure the statistical significance, all calculated values of  $\alpha$  during one season are collected to derive the seasonal-averaged  $\alpha$  profile. Finally, we exclude those separations for which there are fewer than 150 points and calculate  $L$  by performing a least squares fit to each seasonal-averaged  $\alpha$  profile.

Figure 1 indicates the averaged seasonal variations of  $\alpha$  and its dependences on the layer distance for noncontiguous and contiguous cloud layers during 1997–2010 year. Here, we define those nonadjacent layers without clear sky between them as a contiguous cloud pair. Otherwise, they are classified as a noncontiguous cloud pair (Hogan & Illingworth, 2000). For the noncontiguous cloud pair (solid lines in Figure 1), the seasonal and vertical variations of  $\alpha$  with layer distance are small; its values range from 0 to 0.1 and follow the random overlap very well (e.g., Di Giuseppe & Tompkins, 2015; Hogan & Illingworth, 2000). For the contiguous cloud pair (dash lines), we can see that  $\alpha$  gradually decreases from 0.93 to 0.15 with an increasing layer distance. This indicates that contiguous cloud pairs tend to follow the maximum overlap more for a large layer distance, which is consistent with previous studies (e.g., Di Giuseppe & Tompkins, 2015; Hogan & Illingworth, 2000). The seasonal variation of overlap parameter can be related to the atmospheric state and will be discussed in the section 3. Based on the results from Figure 1, the following analysis only focuses on the contiguous cloud pairs. After performing data screening, the contiguous cloud pairs (i.e.,  $0.0 < C_i < 0.5$  and  $0.0 < C_j < 0.5$ ), which are used to retrieve  $\alpha$  and  $L$ , reach 521,738 samples. In section 3, we divide these samples into two different subsets, one for the creation of a regression model of  $L$  (251,524 samples) and the other one for the evaluation of the model (270,214 samples). It is worth further noting that those cloud layer pairs with cloud cover larger than 0.5 (i.e.,  $0.5 < C_i < 1.0$  and  $0.5 < C_j < 1.0$ ) are also included in evaluating the regression method. Thus, this subset eventually includes 630,900 samples (see Figure 5).

## 2.2. Meteorological Reanalysis Data Set

The daily 3-hr meteorological products (zonal wind  $u$ , meridional wind  $v$ , relative humidity  $rh$ , specific humidity  $sh$ , vertical velocity  $\omega$ , and atmospheric temperature  $T$  profiles) from the Modern-Era Retrospective Analysis for Research and Applications Version 2 (MERRA2; Rienecker et al., 2011), which have a gridded resolution of  $0.5^\circ \times 0.625^\circ$ , are used to calculate the wind shear and atmospheric instability between two atmospheric layers over the SGP site. For any two atmospheric layers in each 1-hr averaged cloud cover profile, the wind shear  $dV/dz_{i,j}$  between the layers  $i$  and  $j$  is defined as follows:

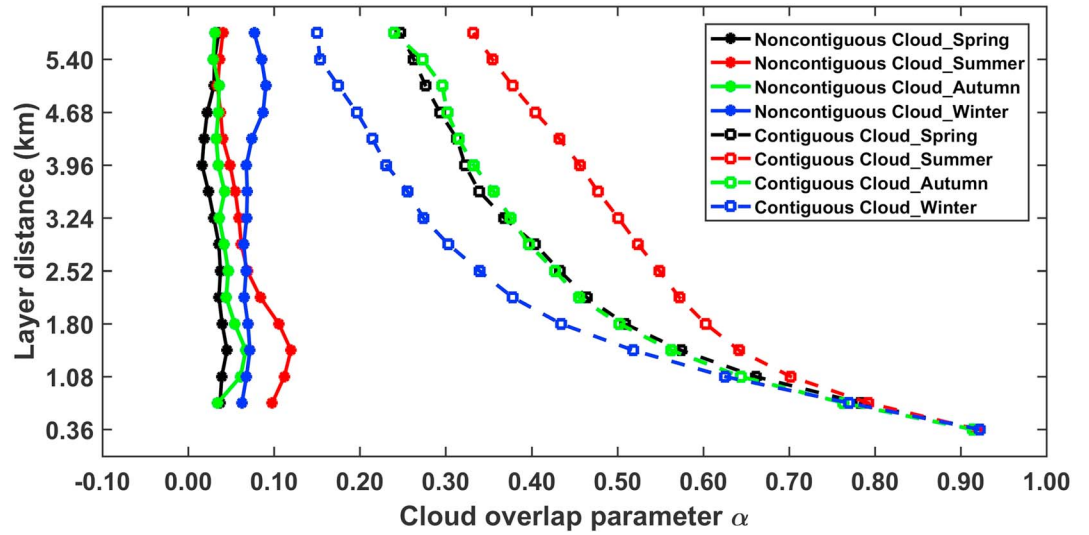


**Figure 1.** The averaged seasonal variations of overlap parameter  $\alpha$  and its dependences on the layer distance for noncontiguous (solid lines) and contiguous cloud layers (dash lines) based on 14-year observations. It is worth noting that those statistical results of  $\alpha$  with layer distance larger than 6 km are excluded due to limited sample numbers.

$$dV/dz_{i,j} = \frac{\max\{V_i; V_j\} - \min\{V_i; V_j\}}{D_{i,j}}, \quad (1)$$

where  $V_i$  and  $V_j$  are the horizontal wind speeds for layers  $i$  and  $j$ , respectively, and  $D_{i,j}$  is the layer separation distance. Similarly, the degree of the conditional instability of the moist convection is expressed as the vertical gradient of the saturated equivalent potential temperature between the same two layers (i.e.,  $\partial\theta_{es}/\partial z_{i,j}$ ). Here,

$$\left\{ \begin{array}{l} \theta_{es} = \theta \exp\left(\frac{L_v r_s}{C_p T}\right), \\ \theta = T \left(\frac{1000}{p}\right)^{0.286}, L_v = 2.5 \times 10^6 - 2323 \times (T - 273.16), \\ r_s = \frac{sh}{rh \times (1 - sh)}, \end{array} \right. \quad (2)$$

where  $\theta$  is the potential temperature,  $P$  is the pressure,  $L_v$  is the latent heat of vaporization,  $C_p$  is the specific heat capacity at a constant pressure,  $r_s$  is the saturation mixing ratio, and  $T$  is the atmospheric temperature. Generally, the larger the  $\partial\theta_{es}/\partial z_{i,j}$ , the more stable the atmosphere. In addition to the wind shear and atmospheric instability, the vertical velocity at 500 hPa, whose positive values are for updrafts and whose negative values are for subsidence, is also analyzed.

### 3. Results and Discussion

#### 3.1. Cloud Overlap Parameterization Based on Dynamical Factors

Based on the method of section 2.1, Figure 2 further provides the time series of seasonal-averaged TCF, decorrelation length scale  $L$ , and their anomalies over the SGP site. Here, the TCFs are derived from different data sources. Based on the cloud profiles of the ARSCLs VAP product, the hourly mean TCF from radar observation is defined as the ratio of cloudy profiles to total sample profiles within a temporal resolution of 1 hr. Thus, the CF\_Radar is the seasonal-averaged value of hourly mean TCFs based on the ARSCLs VAP product. The TCF from the second edition data set of the CLARA (“Cloud, Albedo and Surface Radiation data set from Advanced Very High Resolution Radiometer (AVHRR) data” is also used in this study (hereafter, referred as CF\_CLARA-A2). Here, the CLARA-A2 is the second edition of the Climate Monitoring Satellite Application Facility cloud and radiation data set and is derived from the 34 years of global AVHRR observations onboard the polar-orbiting National Oceanic and Atmospheric Administration and MetOp meteorological satellites (Karlsson et al., 2017). CF\_ERA and CF\_MERRA 2 are derived from ERA-

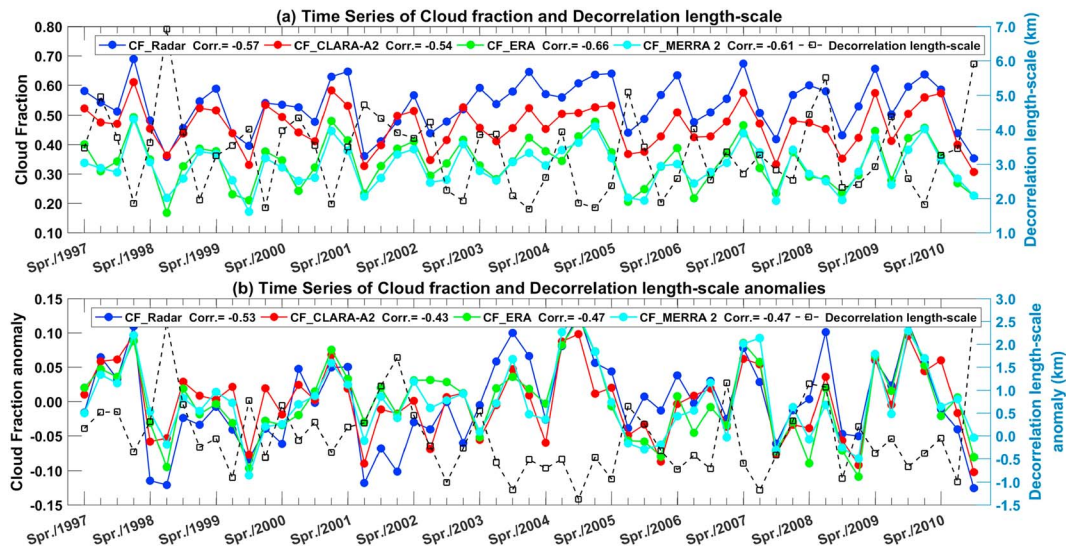


**Figure 2.** Time series (55 seasons) of (a) seasonal-averaged total cloud fraction and decorrelation length scale  $L$  and (b) their anomalies over the SGP site. The correlation coefficients between total cloud fraction from different data sets and  $L$  are also given in the figures. Here, the seasonal-averaged  $L$  that is retrieved based on the cloud layer pairs with cloud cover is smaller than 0.5 (i.e.,  $0.0 < C_i < 0.5$  and  $0.0 < C_j < 0.5$ ), and sample number reaches 521,738. All of the correlation coefficients in this figure ( $Corr.$ ) are the Pearson's rank correlation coefficient. The values of  $P$  calculated using the Student's  $t$  test are smaller than 0.05 ( $P < 0.05$ ).

Interim (Dee et al., 2011) and MERRA2 reanalysis data sets, respectively. In Figure 2, we can see that the seasonal cycles of TCF are consistent for different data sets. However, the difference of cloud fraction seems to be large between them. It possibly refers to the remote sensing method (passive vs. active) and spatial-scale difference (Kennedy et al., 2011). In particular, CF\_CLARA-A2 data set is based on the AVHRR, which is a passive sensor carried by the polar-orbiting satellite. It means that CF\_CLARA-A2 will underestimate the TCF because passive sensors (e.g., MODIS) generally fail to detect the optically thin clouds (optical depth  $< 0.3$ ; Sun et al., 2015). Although CF\_CLARA-A2 data set cannot provide the diurnal cycle of TCF, the TCF difference between CF\_CLARA-A2 and CF\_Radar is impossible caused by the diurnal cycle of TCF because radar observation has revealed the weak diurnal cycle of TCF over the SGP site (e.g., Dong et al., 2006). The underestimations of TCF in CF\_MERRA 2 and CF\_ERA may be due to the fact that these reanalysis products both incorporate satellite data into their assimilation process.

A Student's  $t$  test has been performed for the relationship between TCF and  $L$ . The low  $P$ -values ( $P < 0.05$ ) indicate that the TCFs from four data sets all have significant negative correlation with  $L$ , either their normal value or deseasonalized anomalies. For the normal values of TCF and  $L$ , the correlation coefficients from different TCF data sets range from  $-0.54$  to  $-0.66$  (Figure 2a). Although the correlation coefficients between their anomalies drop to approximately  $-0.45$ , they are still significant (Figure 2b,  $P < 0.05$ ), which means that TCF is sensitive to cloud overlap way, and thus, a reliable parameterization of the  $L$  will contribute to improved simulation of TCF in climate models.

The first question is then how to parameterize  $L$  more reasonably. Naud et al. (2008) pointed out that the sensitivity of  $L$  to the season and location possibly relates to the dynamical process and atmospheric state. Indeed, the annual cycle and long-term series of  $L$  in Figure 3 indicate that its variation is related to the atmospheric states and cloud covers at different layers (i.e.,  $C_i$  and  $C_j$ ). For the annual cycle of  $L$  (Figure 3a), its maximum and minimum values occur during summer and winter seasons, respectively. The cycle is anticorrelated with wind shear and instability. Generally, weaker wind shear and a more unstable atmosphere tend to favor the development of clouds and result in maximum overlap (larger  $L$  values) between cloud layers (Li et al., 2018; Naud et al., 2008), which possibly explains why  $L$  is sensitive to the season.

In addition, because the calculation of overlap factor  $\alpha$  is related to the cloud cover at different levels, an opposite annual cycle between  $L$  and cloud cover can also be seen in Figure 3c. This anticorrelation may be explained by considering an isolated cloud: (1) given a study region, if the cloud cover decreases, then the degree of overlap must increase (Hogan & Illingworth, 2000); (2) if this cloud refers to a strong

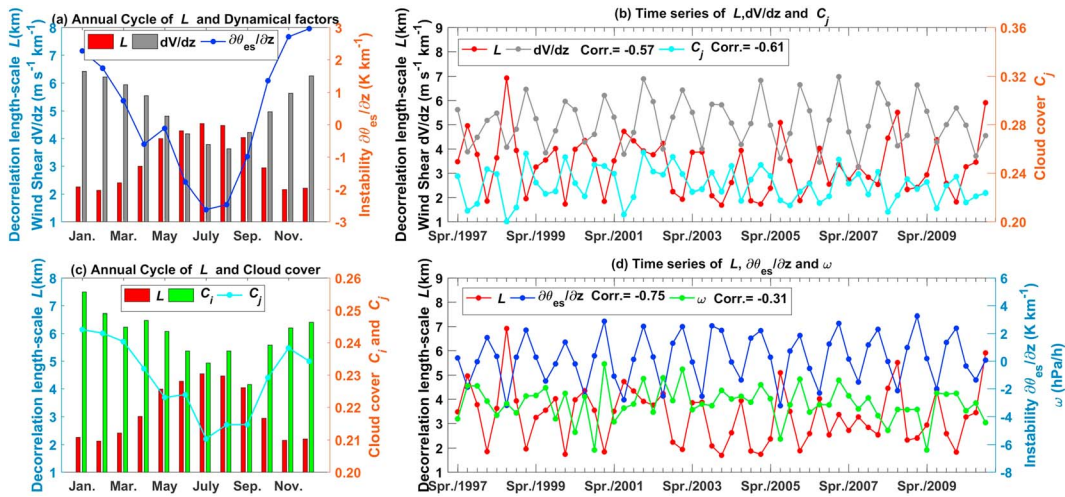


**Figure 3.** (a, c) Annual cycles and (b, d) long-term series of  $L$  and different dynamical factors. The correlation coefficients between  $L$  and dynamical factors series are also given in the figures. All of the correlation coefficients in this figure (*Corr.*) are the Pearson's rank correlation coefficient. The values of  $P$  calculated using the Student's  $t$  test are smaller than 0.05 ( $P < 0.05$ ).

convective system, it tends to develop vertically rather than horizontally and thus results in a smaller cloud cover at a horizontal level. In Figure 3d, it is clear that atmospheric instability exhibits maximum negative correlation with the time series of  $L$  ( $Corr. = -0.75$ ,  $P < 0.05$ ), and wind shear also has obvious correlation with  $L$  ( $Corr. = -0.57$ ,  $P < 0.05$ ). Moreover, only  $C_j$  is obviously negatively correlated with  $L$  and its correlation coefficient reaches  $-0.61$  ( $P < 0.05$ ). Although the annual cycle of vertical velocity does not show correlation with  $L$ , its time series still exhibits significant but weak negative correlation with  $L$  ( $Corr. = -0.31$ ,  $P < 0.05$ ). These statistical relationships are consistent with previous global or regional studies (Di Giuseppe & Tompkins, 2015; Li et al., 2018; Naud et al., 2008). Previous study has pointed out the importance of cloud type to the Earth's climate system and discussed the overlap properties between different cloud types based on the space-based lidar and radar observations (e.g., Li et al., 2015). For the different cloud types, the cloud vertical overlap and its associated impact factor should be different. In this analysis, but, different cloud-type pairs are divided into same group if they have the same layer separation, which causes that the dependence of overlap parameter on cloud type is masked. However, different cloud types refer to different dynamical conditions. As such, deep convective cloud or cumulus tends to occur at an instability atmosphere, whereas status clouds have high occurrence frequency at a stability atmosphere. Thus, this study does not include the information of cloud type and mainly focuses on the dependences of cloud overlap parameters on dynamical factors instead of cloud types. The sensitivity of  $L$  on dynamical parameters found in our study thus still partly reflects the impact of cloud

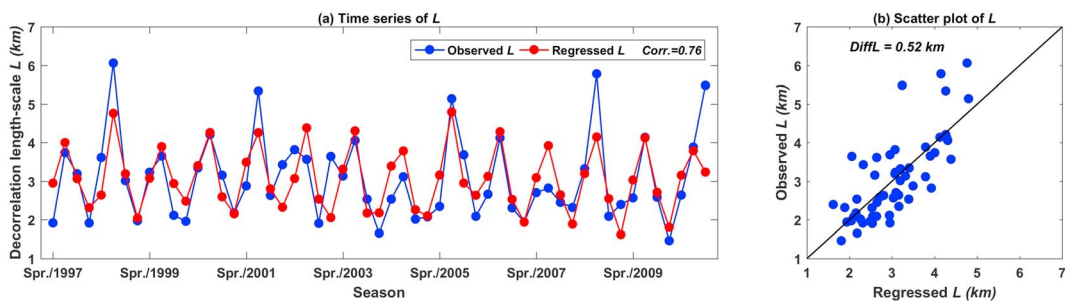


**Figure 4.** (a) Observed and regressed time series (55 seasons) of  $L$  based on the regression model  $L = 3.27 - 0.46 \times \frac{\partial\theta_{es}}{\partial z}$ . The correlation coefficients between observed

and regressed  $L$  are also given in the figure. (b) Similar with (a) but is their scatter plot. Here,  $DiffL = \frac{\sum_{i=1}^{i=55} |L^i_{retrieved} - L^i_{regressed}|}{55}$  and represents the averaged value of absolute differences between retrieved and predicted  $L$ . The correlation coefficient in this figure (*Corr.*) is the Pearson's rank correlation coefficient. The value of  $P$  calculated using the Student's  $t$  test is smaller than 0.05 ( $P < 0.05$ ).

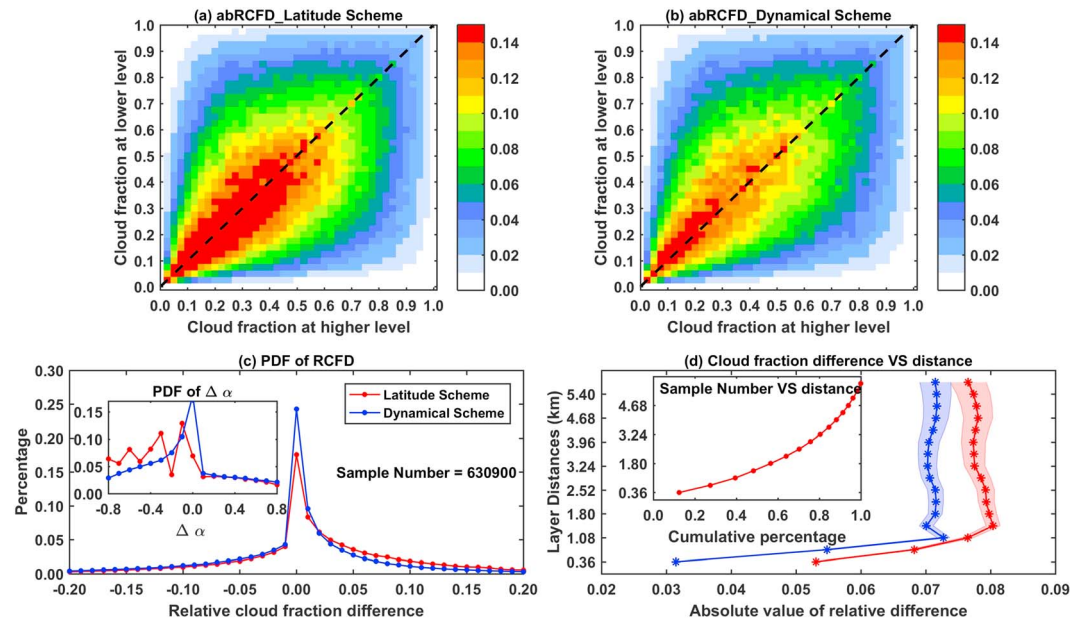


**Figure 5.** Biases of cloud fraction caused by the latitude and dynamical schemes. (a) Absolute value of relative difference (*abRCFD*) between predicted and observed cloud fractions caused by the latitude scheme. (b) Absolute value of relative difference between predicted and observed cloud fractions caused by the dynamical scheme. (c) Probability density functions of relative cloud fraction difference and overlap factor difference (inset in Figure 5c) for the two schemes, with the sample number value (630,900 samples). (d) Variation of *abRCFD* with layer distance; the subplot represents the variation of cumulative percentage of sample number with layer distance. In addition, the color shading represents five standard deviations of the mean.

types on the overlap parameter. However, further researches are needed to study the overlap properties and related impact factor for specific cloud type.

The above analysis indicates that dynamical factors and cloud cover can be regarded as the predictors to build a regression model for  $L$ . Note that the regression model for  $L$  only considers those variables for which their time series show significant correlation with  $L$  (confidence level >95%). After testing the collinearity between different variables, the stepwise regression method is used to filter the predictors and build the optimal regression model. Ultimately, the seasonal data subset (251,524 samples) yields the following model:  $L = 3.27 - 0.46 \times \frac{\partial \alpha}{\partial z}$ . This model captures a significant amount of the variability in  $L$  over the 1997–2010 record (see Figure 4), and the  $R$ -squared values ( $R^2$ ) and averaged value of absolute differences between retrieved

and predicted  $L$  (i.e.,  $\text{Diff}L = \frac{\sum_{i=1}^{i=55} |L^i_{\text{retrieved}} - L^i_{\text{regressed}}|}{55}$ ) for this regression model are 0.57 (correlation coefficient  $\text{Corr.} = 0.76$ ,  $P < 0.05$ ) and 0.52 km, respectively.

In addition, the regression model reveals that atmospheric instability is the primary factor that controls the seasonal cycle of  $L$ , with wind shear and other variables playing an insignificant role over the SGP site. This result is different from previous ones that attempted to parameterize  $L$  as a function of wind shear alone ( $L = 4.4 - 0.45 \times \frac{dV}{dz}$ ; Di Giuseppe & Tompkins, 2015) or wind shear and atmospheric instability ( $L = 2.18 - 0.09 \times \frac{dV}{dz} - 0.15 \times \frac{\partial \alpha}{\partial z}$ ; Li et al., 2018). In the above studies, wind shear is considered as an important factor, but the wind shear effect on cloud overlap varies by as much as a factor of 5 in these two studies. Note that the above wind shear-dependent schemes are either from short-term satellite observations or aim at a specific region. Comparison between them cannot demonstrate which is superior or has universal application. However, the inconsistency between different schemes indicates that the sensitivity of the  $L$  on dynamical factors varies with large-scale meteorological conditions. Indeed, Jing et al. (2018) showed that the vertical velocity-dependent scheme of  $L$  may significantly reduce biases in the cloud fraction and radiation fields in tropical convective regions compared with traditional overlap schemes. However, over the extratropical regions, vertical velocity exhibits a

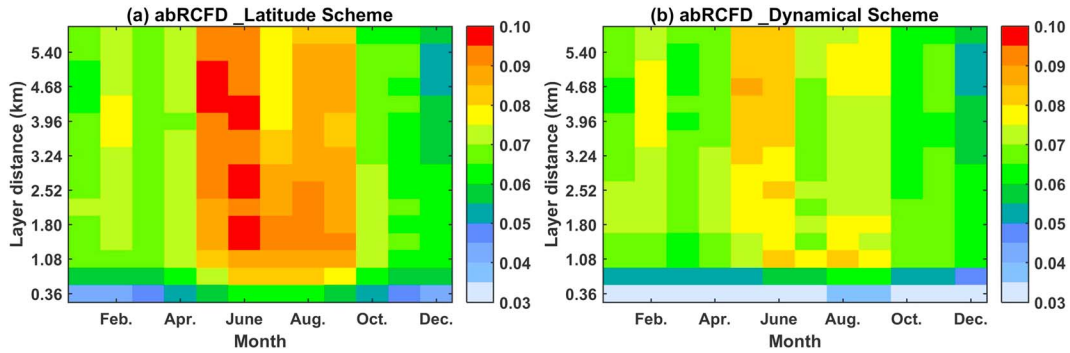


**Figure 6.** The dependence of total cloud fraction biases caused by the different overlap schemes on the layer distance and month; (a) Absolute value of relative difference (*abRCFD*) between predicted and observed cloud fractions for the latitude scheme ( $L = 2.899 - 0.02759 \times |\phi|$ ,  $\phi$  is latitude; Shonk et al., 2010). (b) Absolute value of relative difference between predicted and observed cloud fractions for the dynamical scheme. Here,  $abRCFD = |(CF_{\text{predicted}} - CF_{\text{observed}})/CF_{\text{observed}}|$ .

weak correlation with  $L$ , which is similar to recent statistical results over the Tibetan plateau (Li et al., 2018), and an insignificant contribution to the seasonal cycle of  $L$ .

### 3.2. Comparison Between Different Overlap Parameterization and Contribution Calculation

To assess performance of the new model (hereafter, the dynamical scheme), we calculate the bias of cloud fraction caused by the dynamical scheme (see Figure 5b). The bias is represented by using the absolute value of relative difference between predicted and observed cloud fractions. Here, the relative cloud fraction difference  $RCFD = (CF_{\text{predicted}} - CF_{\text{observed}})/CF_{\text{observed}}$  and its absolute value may be expressed as follows:  $abRCFD = |RCFD|$ . For comparison, the bias of the latitude scheme presented by Shonk et al. (2010) is also presented (Figure 5a). The latitude scheme parameterizes  $L$  as a function of latitude based on the ground-based radar observations ( $L = 2.899 - 0.02759 \times |\phi|$ ,  $\phi$  is latitude) and exhibits smaller TCF bias compared with random and maximum assumptions (Li et al., 2018). However, given the cloud covers at higher and lower atmospheric levels as  $C_i$  and  $C_j$ , we find that the *abRCFD* between these two layers from the latitude scheme even exceeds 15% when  $C_i$  and  $C_j$  have low but similar values (Figure 5a). Compared with the latitude scheme, the dynamical scheme improves the calculation of  $\alpha$  (see Figure S1 in the supporting information) and reduces the cloud fraction bias (Figure 5b). Especially, Figure 6 shows that the improvement of TCF from dynamical scheme is more prominent during the summer season and at small layer distance (e.g., <1 km). Our statistical results further indicate that the *abRCFD* from these two schemes tends to increase with increasing layer distances between two atmospheric layers (Figure 5d). The values of bias range from 3% (5.3%) to approximately 7% (8%) for dynamical (latitude) schemes. On average, the cloud fraction bias caused by the dynamical scheme is always smaller than the *abRCFD* from the latitude scheme, especially for those cloud layers with small separation (e.g., <1 km). When the layer distance exceeds 1 km, the *abRCFD* from these two schemes keeps the values constant. These results verify that the dynamical scheme may further improve the calculation of TCF over the SGP site compared with latitude scheme.

If given the cloud covers at higher and lower atmospheric levels as  $C_i$  and  $C_j$  and  $C_j < C_i$ , the difference between predictions based on any scheme and observed cloud fractions can then be expressed as  $\Delta C = \Delta\alpha \times C_j \times (C_i - 1)$ . It is clear that a negative  $\alpha$  (or  $L$ ) bias will result in a positive cloud fraction bias. Figure 5c indicates that latitude and dynamical schemes have a similar positive  $\alpha$  bias and comparable negative *RCFDs* based on these two schemes. Compared with the latitude scheme, we can see that the dynamical scheme reduces the percentage of underestimation for  $\alpha$  and increases the percentage of no bias and reduces the overestimation of cloud fraction.

Another key question that needs to be answered is which factor dominates the long-term variation of  $L$  over the SGP site. To answer this question, the seasonal anomalies of different predictors based on 521,738 samples, which are already deseasonalized, detrended, and normalized, are used to build the regression relationship. Similarly, we first test the collinearity between different variables (e.g.,  $\Delta C_i, \Delta C_j, \Delta \frac{\partial \omega}{\partial z}, \Delta \frac{dV}{dz}$ , and  $\Delta \omega$ ) and then use the stepwise regression method to remove the insignificant terms from the multilinear models.

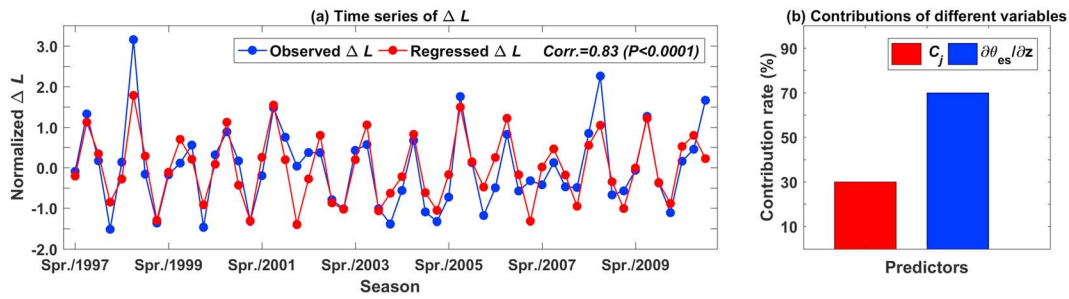


**Figure 7.** (a) Observed and regressed time series of  $\Delta L$  based on all 521,738 samples. (b) Relative contributions of different variables to  $\Delta L$ . Similar with Figure 2;  $\Delta L$  is retrieved based on the cloud layer pairs with cloud cover smaller than 0.5 (i.e.,  $0.0 < C_i < 0.5$  and  $0.0 < C_j < 0.5$ ). The correlation coefficient in this figure (*Corr.*) is the Pearson's rank correlation coefficient. The value of  $P$  calculated using the Student's  $t$  test is smaller than 0.05 ( $P < 0.05$ ).

Finally, we obtain the following model:  $\Delta L = -0.27 \times \Delta C_j - 0.63 \times \Delta \frac{\partial \theta_{es}}{\partial z}$ . The calculation of the relative contributions of different variables to  $\Delta L$  is based on the following equation (Huang & Yi, 1991):

$$RC_j = \frac{1}{m} \sum_{i=1}^m \left[ T_{ij}^2 / \left( \sum_{j=1}^n T_{ij}^2 \right) \right], \quad (3)$$

where  $m$  is the length of the data series and  $n$  is the number of predictors.  $T_{ij} = b_j x_{ij}$ ,  $b_j$  denotes the regression coefficients of each term,  $x_{ij}$  represents predictor variables, and  $j$  is the number of predictor variables.

Figure 7a indicates the agreement between the observed and regressed time series of  $\Delta L$  in which the correlation coefficient reaches 0.83 ( $P < 0.05$ ). This means that the regression model of  $\Delta L$  based on anomalies of cloud cover and instability has the ability to reproduce long-term variations of  $L$ . Based on the contribution calculation, we find that the long-term variation of  $L$  over the SGP site is mainly controlled by the atmospheric instability anomalies and that its contribution reaches 70% (Figure 7b). In addition, it is interesting to see that the variation of cloud cover at lower atmospheric levels (i.e.,  $\Delta C_j$ ) also contributes 30% of  $\Delta L$ , although  $C_j$  has a negligible effect on the seasonal cycle of  $L$ .

#### 4. Summary

TCF has been considered as the key variable modulating the Earth's radiation budget. Recent research has indicated that the contribution of TCF to long-term variation of the planetary albedo (PA) may reach 70% over the oceans at middle and low latitudes (Jian et al., 2018). However, one of the remaining challenges is that atmospheric models have to develop adjustable parameterizations of overlap parameter—decorrelation length scale  $L$ —instead of fixed ones to accurately calculate the TCF. Due to the inability of passive sensors in detecting cloud vertical structure (Chang & Li, 2005a, 2005b; Huang et al., 2005, 2006), this study uses ground-based radar observation to derive the long-term seasonal-averaged  $L$  over the SGP. By matching the meteorological reanalysis data set, we demonstrate that the potential of dynamical variables can be used to develop the adjustable parameterization of  $L$  and find that a dynamical-dependent scheme of  $L$  may reduce the TCF bias over the SGP site compared with the previous one. More importantly, our statistical results show that atmospheric instability is the most important control factor of  $L$  variation over the SGP site, and its contribution even reaches 70%.

The present cloud overlap parameterization only refers to the cloud fraction of nonprecipitating clouds other than in-cloud properties. If we further focus on the vertical alignment of highly variable in-cloud microphysical properties, the cloud fraction overlap needs to be replaced by a probability density function (PDF) overlap of in-cloud and precipitation properties (e.g., cloud liquid and ice, rain, and snow; Ovchinnikov et al., 2016). Although cloud radiative effect bias caused by above PDF overlap is proven to be quarter to half of the bias from cloud fraction overlap, the uncertainty in PDF overlap scheme still is nonnegligible (Wang, 2017). Recent study further points out that hydrometeor fall speeds can be used to improve the representation of vertical alignment of cloud and precipitation properties and develop PDF overlap parameterization in climate models (Ovchinnikov et al., 2019). Above studies and our result thus suggest that the effects of

dynamical variables should be considered in the parameterizations of either cloud fraction overlap or PDF overlap to improve the calculation of radiative budget and further reduce the uncertainties in projection of future climate.

In fact, the related methods used to calculate  $L$  and quantify the relative contributions can also be used at other ARM sites. However, the chief goal of this study is not to develop a superior or universal parameterization of  $L$  but to demonstrate the potential of dynamical-dependent parameterization and further quantify the contribution of different dynamical factors to long-term variation of  $L$  over SGP site. Thus, the parameterization of  $L$  derived from SGP site is not always feasible for other climate regimes, and dominant contribution factor of long-term variation of  $L$  also varies with regions. The varied sensitivity may be caused by different factors. First, besides cloud dynamics, other variables (e.g., cloud microphysical properties) also play a non-negligible role in determining cloud overlap properties (Heymsfield, 1972). Second, present study cannot entirely remove the effect of data truncation on the calculation of  $L$  by using a simple sample filter. The variation of cloud system scale with region and height may result in different retrieval bias of  $L$  if given the temporal resolution (or sampling scale). However, the retrieval uncertainty of  $L$  could be reduced using global statistics of cloud system scales as a function of dynamical factors (Guillaume et al., 2018), and a more robust parameterization of  $L$  will be built.

#### Acknowledgments

This research was jointly supported by the Foundation for Innovative Research Groups of the National Science Foundation of China (Grant 41521004) and the National Science Foundation of China (Grants 41575015 and 91837204). The authors declare that they have no conflict of interest. We would like to thank the Atmospheric Radiation Measurement Program sponsored by the U.S. Department of Energy and MERRA2 science teams for providing excellent and accessible data products. The ARSCLs data set is available from this link (<http://www.archive.arm.gov/discovery/#v/home/s/>), and MERRA2 daily product may be accessed from this link (<https://disc.gsfc.nasa.gov/datasets/>).

#### References

- Ackerman, T. P., & Stokes, G. M. (2003). The atmospheric radiation measurement program. *Physics Today*, 56(1), 38–44. <https://doi.org/10.1063/1.1554135>
- Barker, H. W. (2008). Overlap of fractional cloud for radiation calculations in GCMs: A global analysis using CloudSat and CALIPSO data. *Journal of Geophysical Research*, 113, D00A01. <https://doi.org/10.1029/2007JD009677>
- Barker, H. W., Stephens, G. L., & Fu, Q. (1999). The sensitivity of domain-averaged solar fluxes to assumptions about cloud geometry. *Quarterly Journal of the Royal Meteorological Society*, 125(558), 2127–2152. <https://doi.org/10.1002/qj.49712555810>
- Boucher, O., Randall, D., Artaxo, P., Bretherton, C., Feingold, G., Forster, P., et al. (2013). In T. F. Stocker, D. Qin, G.-K. Plattner, M. Tignor, S. K. Allen, J. Boschung, A. Nauels, Y. Xia, V. Bex, & P. M. Midgley (Eds.), *Clouds and aerosols, in: Climate Change 2013: The physical science basis. Contribution of working group I to the fifth assessment report of the intergovernmental panel on climate change* (pp. 571–657). Cambridge, UK, New York: Cambridge University Press. <https://doi.org/10.1017/CBO9781107415324>
- Chang, F. L., & Li, Z. (2005a). A new method for detection of cirrus overlapping-low clouds and determination of their optical properties. *Journal of the Atmospheric Sciences*, 62(11), 3993–4009. <https://doi.org/10.1175/JAS3578.1>
- Chang, F. L., & Li, Z. (2005b). A near global climatology of single-layer and overlapped clouds and their optical properties retrieved from TERRA/MODIS data using a new algorithm. *Journal of Climate*, 18(22), 4752–4771. <https://doi.org/10.1175/JCLI3553.1>
- Clothiaux, E. E., Ackerman, T. P., Mace, G. G., Moran, K. P., Marchand, R. T., Miller, M. A., & Martner, B. E. (2000). Objective determination of cloud heights and radar reflectivities using a combination of active remote sensors at the ARM CART sites. *Journal of Applied Meteorology and Climatology*, 39, 645–665. [https://doi.org/10.1175/1520-0450\(2000\)039<0645:ODOCHA>2.0.CO;2](https://doi.org/10.1175/1520-0450(2000)039<0645:ODOCHA>2.0.CO;2)
- Dee, D. P., Uppala, S. M., Simmons, A. J., Berrisford, P., Poli, P., Kobayashi, S., et al. (2011). The ERA-Interim reanalysis: Configuration and performance of the data assimilation system. *Quarterly Journal of the Royal Meteorological Society*, 137(656), 553–597. <https://doi.org/10.1002/qj.828>
- Di Giuseppe, F., & Tompkins, A. M. (2015). Generalizing cloud overlap treatment to include the effect of wind shear. *Journal of the Atmospheric Sciences*, 72(8), 2865–2876. <https://doi.org/10.1175/JAS-D-14-0277.1>
- Dong, X., & Mace, G. G. (2003). Arctic stratus cloud properties and radiative forcing derived from ground-based data collected at Barrow, Alaska. *Journal of Climate*, 16(3), 445–461. [https://doi.org/10.1175/1520-0442\(2003\)016<0445:ASCPAR>2.0.CO;2](https://doi.org/10.1175/1520-0442(2003)016<0445:ASCPAR>2.0.CO;2)
- Dong, X., Xi, B., & Minnis, P. (2006). A climatology of midlatitude continental clouds from the ARM SGP central facility: Part II. Cloud fraction and surface radiative forcing. *Journal of Climate*, 19(9), 1765–1783. <https://doi.org/10.1175/JCLI3710.1>
- Geleyn, J. F., & Hollingsworth, A. (1979). An economical analytical method for the computation of the interaction between scattering and line absorption of radiation. *Contributions to Atmospheric Physics*, 10(3), 826–841. <https://doi.org/10.1002/2017MS001190>
- Guillaume, A., Kahn, B. H., Yue, Q., Fetzer, E. J., Wong, S., Manion, G. J., et al. (2018). Horizontal and vertical scaling of cloud geometry inferred from CloudSat data. *Journal of the Atmospheric Sciences*, 75(7), 2187–2197. <https://doi.org/10.1175/JAS-D-17-0111.1>
- Heymsfield, A. (1972). Ice crystal terminal velocities. *Journal of the Atmospheric Sciences*, 29, 1348–1357. [https://doi.org/10.1175/1520-0469\(1972\)0291348:ICTV.2.0.CO;2](https://doi.org/10.1175/1520-0469(1972)0291348:ICTV.2.0.CO;2)
- Hogan, R. J., & Illingworth, A. J. (2000). Deriving cloud overlap statistics from radar. *Quarterly Journal of the Royal Meteorological Society*, 126(569), 2903–2909. <https://doi.org/10.1002/qj.49712656914>
- Huang, J., Guo, J., Wang, F., Liu, Z., Jeong, M.-J., Yu, H., & Zhang, Z. (2015). CALIPSO inferred most probable heights of global dust and smoke layers. *Journal of Geophysical Research: Atmospheres*, 120, 5085–5100. <https://doi.org/10.1002/2014JD022898>
- Huang, J., & Yi, Y. (1991). Inversion of a nonlinear dynamical model from the observation. *Science in China*, 34B, 1246–1251.
- Huang, J. P., Minnis, P., & Lin, B. (2005). Advanced retrievals of multilayered cloud properties using multispectral measurements. *Journal of Geophysical Research*, 110, D15S18. <http://doi.org/10.1029/2004JD005101>
- Huang, J. P., Minnis, P., & Lin, B. (2006). Determination of ice water path in ice-over-water cloud systems using combined MODIS and AMSR-E measurements. *Geophysical Research Letters*, 33, L21801. <http://doi.org/10.1029/2006GL027038>
- Jian, B., Li, J., He, Y., Wang, G., Zhang, M., & Huang, J. (2018). The impacts of atmospheric and surface parameters on long-term variations in the planetary albedo. *Journal of Climate*, 31(21), 8705–8718. <https://doi.org/10.1175/JCLI-D-17-0848.1>
- Jing, X. W., Zhang, H., Satoh, M., & Zhao, S. Y. (2018). Improving representation of tropical cloud overlap in GCMs based on cloud-resolving model data. *Journal of Meteorological Research*, 32(2), 233–245. <https://doi.org/10.1007/s13351-018-7095-9>

- Karlsson, K.-G., Anttila, K., Trentmann, J., Stengel, M., Meirink, J. F., Devasthale, A., et al. (2017). CLARA-A2: The second edition of the CM SAF cloud and radiation data record from 34 years of global AVHRR data. *Atmospheric Chemistry and Physics*, *17*(9), 5809–5828. <https://doi.org/10.5194/acp-17-5809-2017>
- Kennedy, A. D., Dong, X. Q., Xi, B. K., Xie, S. C., Zhang, Y. Y., & Chen, J. Y. (2011). A comparison of MERRA and NARR reanalyses with the DOE ARM SGP data. *Journal of Climate*, *24*(17), 4541–4557. <https://doi.org/10.1175/2011JCLI3978.1>
- Li, J., Huang, J., Stamnes, K., Wang, T., Lv, Q., & Jin, H. (2015). A global survey of cloud overlap based on CALIPSO and CloudSat measurements. *Atmospheric Chemistry and Physics*, *15*(1), 519–536. <https://doi.org/10.5194/acp-15-519-2015>
- Li, J., Lv, Q., Jian, B., Zhang, M., Zhao, C., Fu, Q., et al. (2018). The impact of atmospheric stability and wind shear on vertical cloud overlap over the Tibetan Plateau. *Atmospheric Chemistry and Physics*, *18*(10), 7329–7343. <https://doi.org/10.5194/acp-18-7329-2018>
- Mace, G. G., & Benson Troth, S. (2002). Cloud-layer overlap characteristics derived from Long-term cloud radar data. *Journal of Climate*, *15*(17), 2505–2515. [https://doi.org/10.1175/1520-0442\(2002\)015<2505:CLOCDF>2.0.CO;2](https://doi.org/10.1175/1520-0442(2002)015<2505:CLOCDF>2.0.CO;2)
- Mace, G. G., Zhang, Q., Vaughan, M., Marchand, R., Stephens, G., Trepte, C., & Winker, D. (2009). A description of hydrometeor layer occurrence statistics derived from the first year of merged CloudSat and CALIPSO data. *Journal of Geophysical Research*, *114*, D00A26. <https://doi.org/10.1029/2007JD009755>
- Morcrette, J. J., & Fouquart, Y. (1986). The overlapping of cloud layers in shortwave radiation parameterizations. *Journal of the Atmospheric Sciences*, *43*(4), 321–328. [https://doi.org/10.1175/1520-0469\(1986\)043<0321:TOOCL>2.0.CO;2](https://doi.org/10.1175/1520-0469(1986)043<0321:TOOCL>2.0.CO;2)
- Morcrette, J. J., & Jakob, C. (2000). The response of the ECMWF model to changes in the cloud overlap assumption. *Monthly Weather Review*, *128*(6), 1707–1732. [https://doi.org/10.1175/1520-0493\(2000\)128<1707:TROTEM>2.0.CO;2](https://doi.org/10.1175/1520-0493(2000)128<1707:TROTEM>2.0.CO;2)
- Naud, C. M., del Genio, A., Mace, G. G., Benson, S., Clothiaux, E. E., & Kollias, P. (2008). Impact of dynamics and atmospheric state on cloud vertical overlap. *Journal of Climate*, *21*(8), 1758–1770. <https://doi.org/10.1175/2007JCLI1828.1>
- Oreopoulos, L., & Norris, P. M. (2011). An analysis of cloud overlap at a midlatitude atmospheric observation facility. *Atmospheric Chemistry and Physics*, *11*(12), 5557–5567. <https://doi.org/10.5194/acp-11-5557-2011>
- Ovchinnikov, M., Giangrande, S., Larson, V. E., Protat, A., & Williams, C. R. (2019). Dependence of vertical alignment of cloud and precipitation properties on their effective fall speeds. *Journal of Geophysical Research: Atmospheres*, *124*, 2079–2093. <https://doi.org/10.1029/2018JD029346>
- Ovchinnikov, M., Lim, K. S. S., Larson, V. E., Wong, M., Thayer-Calder, K., & Ghan, S. J. (2016). Vertical overlap of probability density functions of cloud and precipitation hydrometeors. *Journal of Geophysical Research: Atmospheres*, *121*, 12,966–12,984. <https://doi.org/10.1002/2016JD025158>
- Pincus, R., Hannay, C., Klein, S. A., Xu, K. M., & Hemler, R. (2005). Overlap assumptions for assumed probability distribution function cloud schemes in large-scale models. *Journal of Geophysical Research*, *110*, D15S09. <https://doi.org/10.1029/2004JD005100>
- Rienecker, M. M., Suarez, M. J., Gelaro, R., Todling, R., Bacmeister, J., Liu, E., et al. (2011). MERRA: NASA's modern-era retrospective analysis for research and applications. *Journal of Climate*, *24*(14), 3624–3648. <https://doi.org/10.1175/JCLI-D-11-00015.1>
- Seinfeld, J. H., Bretherton, C., Carslaw, K. S., Coe, H., DeMott, P. J., Dunlea, E. J., et al. (2016). Improving our fundamental understanding of the role of aerosol-cloud interactions in the climate system. *Proceedings of the National Academy of Sciences*, *113*(21), 5781–5790. <https://doi.org/10.1073/pnas.1514043113>
- Shonk, J. K., Hogan, R. J., Edwards, J. M., & Mace, G. G. (2010). Effect of improving representation of horizontal and vertical cloud structure on the Earth's global radiation budget. Part I: Review and parametrization. *Quarterly Journal of the Royal Meteorological Society*, *136*(650), 1191–1204. <https://doi.org/10.1002/qj.647>
- Stephens, G. L. (2005). Cloud feedbacks in the climate system: A critical review. *Journal of Climate*, *18*(2), 237–273. <https://doi.org/10.1175/JCLI-3243.1>
- Stephens, G. L., Wood, N. B., & Gabriel, P. M. (2004). An assessment of the parameterization of subgrid-scale cloud effects on radiative transfer. Part I: Vertical overlap. *Journal of the Atmospheric Sciences*, *61*, 715–732. [https://doi.org/10.1175/1520-0469\(2004\)061<0715:AAOTPO>2.0.CO;2](https://doi.org/10.1175/1520-0469(2004)061<0715:AAOTPO>2.0.CO;2)
- Sun, W., Baize, R. R., Videen, G., Hu, Y., & Fu, Q. (2015). A method to retrieve super-thin cloud optical depth over ocean background with polarized sunlight. *Atmospheric Chemistry and Physics*, *15*(20), 11,909–11,918. <https://doi.org/10.5194/acp-15-11909-2015>
- Tompkins, A., & Giuseppe, F. D. (2015). An interpretation of cloud overlap statistics. *Journal of the Atmospheric Sciences*, *72*(8), 2877–2889. <https://doi.org/10.1175/JAS-D-14-0278.1>
- Wang, X. C. (2017). Effects of cloud condensate vertical alignment on radiative transfer calculations in deep convective regions. *Atmospheric Research*, *186*, 107–115. <https://doi.org/10.1016/j.atmosres.2016.11.014>
- Wang, X. C., Liu, Y. M., & Bao, Q. (2016). Impacts of cloud overlap assumptions on radiative budgets and heating fields in convective regions. *Atmospheric Research*, *167*, 89–99. <https://doi.org/10.1016/j.atmosres.2015.07.017>
- Weger, R. C., Lee, J., Zhu, T., & Welch, R. M. (1992). Clustering, randomness and regularity in cloud fields: 1. Theoretical considerations. *Journal of Geophysical Research*, *97*(D18), 20,519–20,536. <https://doi.org/10.1029/92JD02038>
- Willén, U., Crewell, S., Baltink, H. K., & Sievers, O. (2005). Assessing model predicted vertical cloud structure and cloud overlap with radar and lidar ceilometer observations for the Baltex Bridge Campaign of CLIWA-NET. *Atmospheric Research*, *75*(3), 227–255. <https://doi.org/10.1016/j.atmosres.2004.12.008>
- Zhao, W., Marchand, R., & Fu, Q. (2017). The diurnal cycle of clouds and precipitation at the ARM SGP site: Cloud radar observations and simulations from the multiscale modeling framework. *Journal of Geophysical Research: Atmospheres*, *122*, 7519–7536. <https://doi.org/10.1002/2016JD026353>